

This work was written as part of one of the author's official duties as an Employee of the United States Government and is therefore a work of the United States Government. In accordance with 17 U.S.C. 105, no copyright protection is available for such works under U.S. Law.

Public Domain Mark 1.0

<https://creativecommons.org/publicdomain/mark/1.0/>

Access to this work was provided by the University of Maryland, Baltimore County (UMBC) ScholarWorks@UMBC digital repository on the Maryland Shared Open Access (MD-SOAR) platform.

Please provide feedback

Please support the ScholarWorks@UMBC repository by emailing scholarworks-group@umbc.edu and telling us what having access to this work means to you and why it's important to you. Thank you.

Low-Frequency Oscillations in Optical Measurements of Metal-Nanoparticle Vibrations

Aftab Ahmed,* Rachel Gelfand, S. David Storm, Anna Lee, Anna Klinkova, Jeffrey R. Guest,* and Matthew Pelton*



Cite This: *Nano Lett.* 2022, 22, 5365–5371



Read Online

ACCESS |



Metrics & More



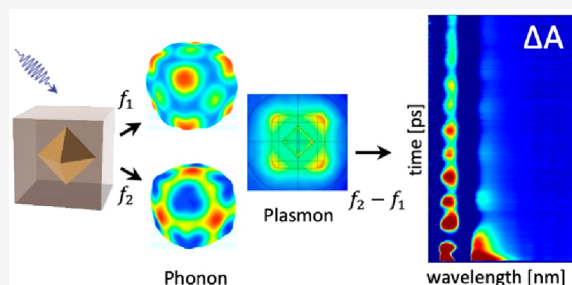
Article Recommendations



Supporting Information

ABSTRACT: Time-resolved optical measurements of vibrating metal nanoparticles have been used extensively to probe the ultrafast mechanical properties of the nanoparticles and of the surrounding liquid, but nearly all investigations so far have been limited to the linear regime. Here, we report the observation of a low-frequency oscillating signal in transient-absorption measurements of nanoparticles with octahedral gold cores and cubic silver shells; the signal appears at the difference of two mechanical vibrational frequencies in the particles, suggesting a nonlinear mixing process. We tentatively attribute this proposed mixing to a nonlinear coupling between a vibrational mode of the nanoparticle and its optical-frequency plasmon resonance. The optimization of this nonlinear transduction may enable high-efficiency opto-mechanical frequency mixing in the GHz–THz frequency regime.

KEYWORDS: Nonlinear mixing, transient absorption, acoustic vibrations, phonon oscillations, time-resolved spectroscopy



Nonlinear properties of microelectromechanical and nanoelectromechanical systems (MEMSs and NEMSs, respectively) have been extensively investigated over the past two decades, both for the limitations they impose on conventional applications such as sensing, frequency generation, and switching, and for the unconventional applications they may enable.^{1,2} Nonlinearities in individual MEMS resonators can arise from a multitude of effects, including a nonlinear relationship between strain and amplitude (known as a geometrical nonlinearity),³ nonlinear elastic forces in the materials that make up the resonators, and nonlinear electrostatic, electromagnetic, or piezoelectric actuation (including parametric actuation).⁴ These nonlinearities, in turn, can induce coupling between different mechanical modes of the resonators,^{5,6} frequency mixing between different modes,⁷ mechanical frequency-comb generation,^{8,9} self-sustained oscillation,¹⁰ and synchronization of the oscillators.¹¹

Scaling the dimensions of vibrating structures down to the nanoscale increases their resonance frequencies, potentially enabling nonlinear mechanics to move into the GHz and THz frequency ranges. Electronic driving and read-out methods, such as piezoelectric or capacitive transduction, are not feasible for objects where all three dimensions are at the nanometer scale; however, nanoparticle vibrations can be measured using hands-off optical measurements such as Raman scattering,^{12–17} four-wave mixing,^{18,19} and transient-absorption (TA) spectroscopy.^{20–24} TA experiments using metal nanoparticles, in particular, provide sensitive time-domain measurements of

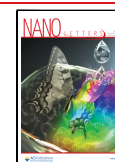
nanoparticle vibration, because of the strong coupling between plasmon resonances and mechanical deformation.²⁵ In these measurements, an ultrafast pump laser pulse heats the nanoparticles, and the resulting thermal expansion coherently excites the vibrational modes. These vibrations induce oscillations in the frequency of plasmon resonances in the nanoparticles, and the oscillating optical properties are measured through changes in the extinction of an ultrafast probe pulse. These measurements have provided detailed information about the mechanical properties of the metal nanoparticles themselves²⁶ and of surrounding liquids.^{27–32}

So far, nearly all measurements of nanoparticle vibrations have been in the linear regime. One exception is a four-wave mixing measurement on small gold nanoparticles vibrating in water; this experiment showed a rapid increase in measured signal above a threshold driving power,³³ which was attributed to cavitation in the surrounding liquid.³⁴ TA measurements on single-walled carbon nanotubes showed modulation of one phonon mode by another, which was attributed to exciton-induced coupling between the modes.³⁵ Here, we report a novel observation of a nonlinear effect in TA measurements of

Received: April 2, 2022

Revised: June 8, 2022

Published: June 14, 2022



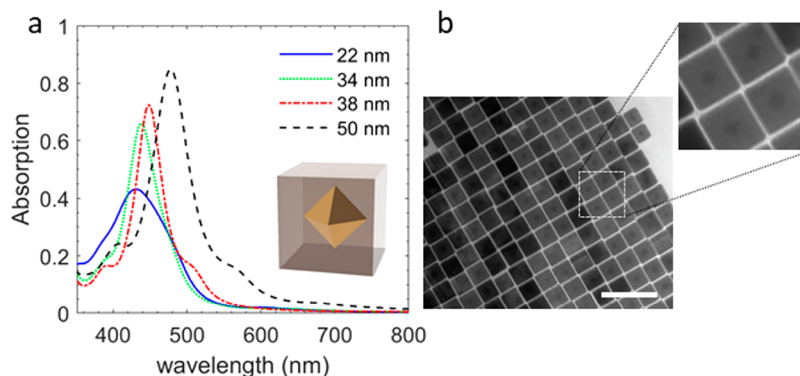


Figure 1. Core-shell nanocubes. (a) Measured extinction spectra for core-shell nanocubes with octahedral gold cores and cubic silver shells. Spectra are measured for particles with shells whose edge lengths range from 22 to 50 nm. The inset shows a schematic of the nanoparticle geometry. (b) Transmission electron microscope images of core-shell nanocubes with 50 nm edge lengths. The scale bar is 100 nm. The gold cores are visible in the higher-magnification image.

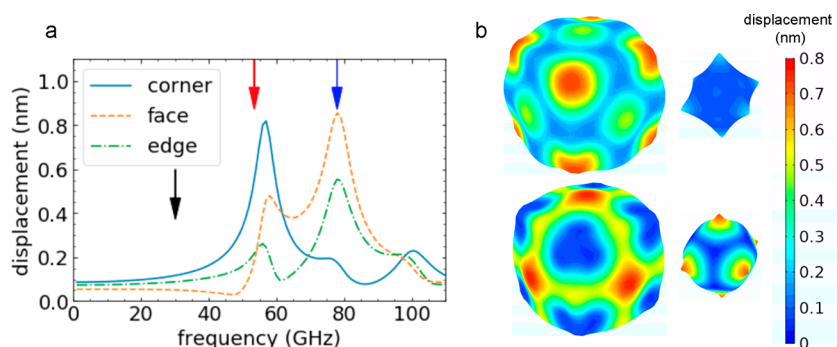


Figure 2. Vibrational modes of core-shell nanocubes. (a) Simulated vibrational spectrum for a core-shell nanocube with an edge length of 38 nm. The plots show the maximum displacement at different points on the surface of the particle as the particle vibrates; the solid blue line is for the corner of the cube; the dashed orange line is for the center of the face of the cube, and the dashed-dotted green line is for the middle of the edge of the cube. Arrows show the experimentally measured oscillation frequencies. (b) Simulated deformations of the core and shell of the nanoparticle for the two dominant vibrational modes of the 38 nm core-shell nanocube, corresponding to the peaks in the vibrational spectrum at 57 GHz (top) and 78 GHz (bottom). Deformations are exaggerated in the renderings. The color scale corresponds to the local displacement from equilibrium in the nanoparticle.

vibrating metal nanoparticles: the appearance of an oscillating signal at the difference frequency between two mechanical modes.

In this work, we study nanoparticles with an octahedral gold core surrounded by a cubic silver shell. These core-shell nanocubes are chemically synthesized by stepwise reduction of metal salt precursors in aqueous solutions of cationic surfactants.³⁶ Shape control of the nanostructure is achieved by adjusting the reaction kinetics and through the use of anions with affinity to specific crystallographic facets.³⁷ (Details about the nanoparticle synthesis are provided in the [SI Methods](#) section.) The cores of the particles are all 16 ± 2 nm, and the shells are grown out to various sizes with cube edge lengths ranging from 22 to 50 nm. [Figure 1a](#) shows the linear extinction spectra of the core-shell nanocubes, and [Figure 1b](#) shows transmission electron microscope (TEM) images of a representative sample. The absorption spectra are similar to those of silver-only cubes with the same edge lengths.³⁸

Previous optical measurements and calculations for silver-nanocube vibrations show that the vibrational spectrum is dominated by two breathing modes; the lower-frequency mode is primarily associated with the motion of the corners of the cubes, and the higher-frequency mode is primarily associated with the motion of the faces of the cubes.^{39–41} We calculated the vibrational modes of our core-shell nanocubes using the

finite-element method and found the same two breathing modes with similar vibrational frequencies as for the silver-only nanocubes. (Details of the finite-element simulations are given in the [SI Methods](#) section.) Representative results are shown in [Figure 2](#) for a core-shell nanocube with an edge length of 38 nm; for this nanoparticle size, the expected vibrational frequencies are 57 and 78 GHz.

We used TA measurements to monitor these vibrations.^{42–44} (Details are given in the [SI Methods](#).) [Figure 3a](#) shows representative results for core-shell nanocubes with 38 nm edge lengths. For all wavelengths, oscillations are seen due to the nanoparticle vibrations on top of the decaying signals due to cooling of the electrons that were initially heated by the incident laser pulse (at short times) and cooling of the nanoparticle lattice to ambient temperature (at longer times). At a probe wavelength of 470 nm, the oscillating signal has a frequency of 54 GHz, in good agreement with the predicted frequency for the lowest-order breathing mode of the nanoparticles (see [Figure 3b](#)). However, at a probe wavelength of 530 nm, the oscillating signal is at a frequency of 29 GHz, significantly lower than the lowest vibrational frequency for the particle (see [Figure 2a](#)). Similar low-frequency oscillations are seen in the TA measurements for core-shell nanocubes of different sizes (see [Figure S1](#)); in all cases, an oscillation is

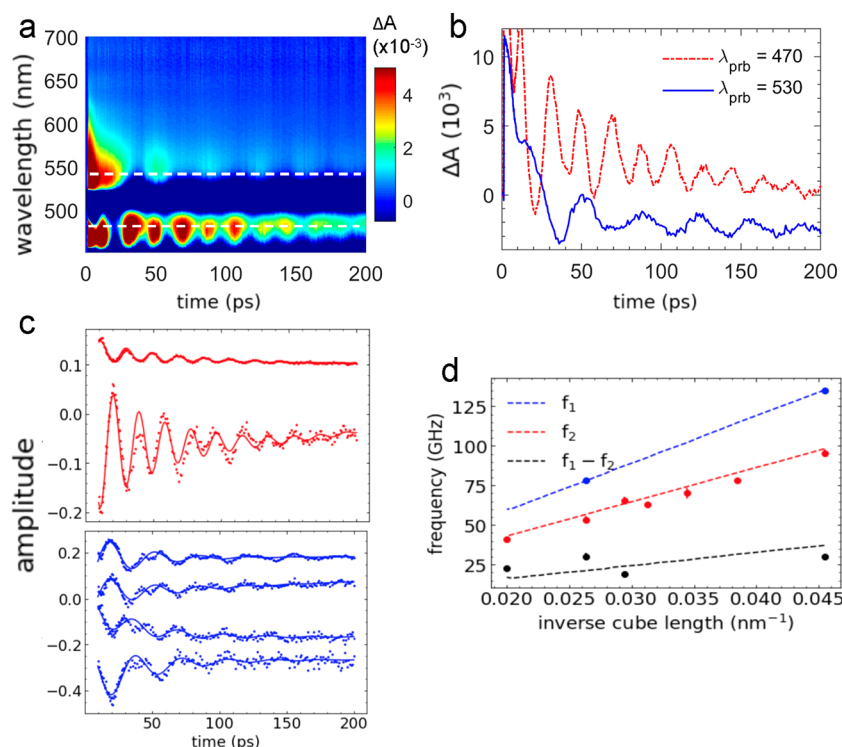


Figure 3. Transient-absorption measurements. (a) Change in the extinction of a probe pulse, ΔA , by an ensemble of core–shell nanocubes with an edge length of 38 nm, as a function of probe frequency and of pump–probe time delay. The large negative signal at probe wavelengths around 510 nm is due to pump-pulse scattering. (b) Transient kinetics for probe wavelengths, λ_{prb} , of 470 and 530 nm (indicated by dashed lines in (a)). (c) Principal kinetics obtained from principal component analysis of the transient-absorption data in (a). Points are experimental principal kinetics, and lines are fits to the decaying oscillations. The kinetics have been separated into two groups (upper and lower panel); within each group, all the kinetics have approximately the same oscillation frequency. (d) Frequencies of oscillations obtained from transient-absorption measurements of vibrating core–shell nanocubes as a function of the inverse edge length. Points are experimental values determined by fitting principal kinetics for several measurements on different particles, for different pump powers, and for different pump wavelengths. Dashed red and blue lines are simulated frequencies, f_1 and f_2 , for the two lowest-order vibrational modes; the dashed black line is the difference between these simulated frequencies.

observed at a frequency lower than that of any vibrational mode of the particle.

To the best of our knowledge, similar low-frequency oscillations have not previously been reported for TA measurements of silver nanocubes³⁹ or of core–shell metal nanoparticles.^{45–51} One exception is the observation of a 16 GHz signal for a single 35 nm silver nanocube on a substrate;⁴¹ in this case, the low-frequency signal was attributed to nanoparticle–substrate interactions. For our measurements, the nanoparticles are measured as a dilute colloidal suspension, so substrate interactions are absent. Previous simulations indicated that the nonuniform heating of larger silver nanocubes excited modes with frequencies below that of the lowest-order breathing mode;³⁹ however, the frequencies of these modes were still higher than those of the low-frequency oscillations observed experimentally in this work.

To systematically identify the frequency components present in the TA data, we analyzed the data using principal component analysis (PCA; see the [SI Methods](#) section for details). This method returns multiple principal kinetics, illustrated in [Figure 3c](#) for the case of the 38 nm core–shell nanocubes. In this case, the principal kinetics cluster in two groups, one with frequencies near 54 GHz and the other with frequencies near 29 GHz. A similar clustering of frequencies into two or three groups is observed for different pump-pulse powers, different pump wavelengths, and different nanocube sizes. The frequencies of these groups are summarized in

[Figure 3d](#), with points representing the average frequency of a group and error bars representing the variation in frequencies within a group (95% confidence interval); full results are given in [Table S1](#). A comparison of these measured frequencies to the results of finite-element simulations clearly shows oscillating TA signals corresponding to the frequencies of the two lowest-order breathing modes of the nanoparticles as well as a slower oscillation whose frequency is consistent with the difference between the two vibrational frequencies. The PCA also shows that the different frequency components, although they show up most clearly at particular probe wavelengths (see [Figure 3b](#)), are present in a wide range of probe wavelengths centered around the plasmon resonance wavelength. We note that, qualitatively, we observe oscillations corresponding to the expected breathing-mode vibrations and difference frequencies in all the measurements; however, in some cases, the signal-to-noise ratio of the TA data is insufficient to allow for a high-quality fit of the principal kinetics and a quantitative determination of the oscillation frequency.

It is unlikely that the observed low-frequency signal comes from mechanical vibrations of larger particles in the sample. If this were the case, the particles would need to have approximately twice the edge length of the average particles; however, TEM images show monodisperse samples with no sign of larger particles. Moreover, the absorption spectrum of the sample does not show evidence for such a population of larger particles, and the synthesis method used to produce the

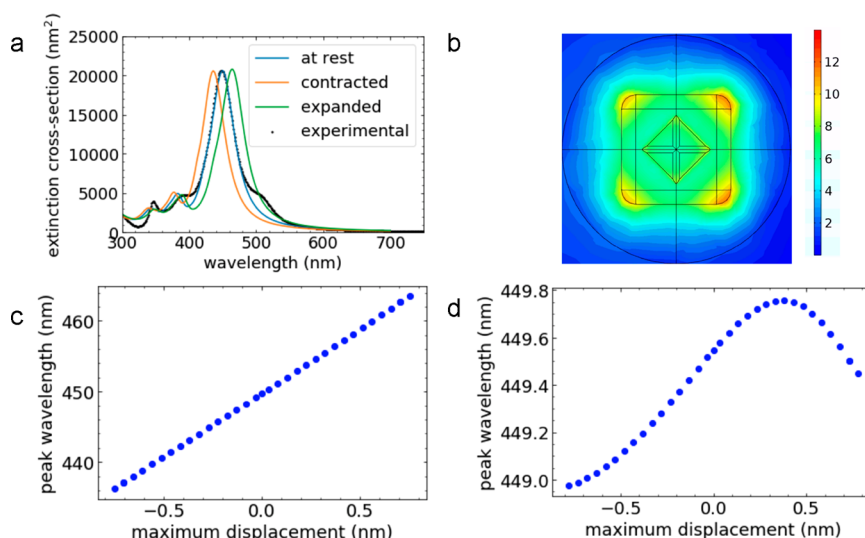


Figure 4. Nonlinear shift in plasmon frequency for the vibrating nanoparticle. (a) Calculated extinction spectra of a core–shell nanocube with an edge length of 38 nm for the nanoparticle at rest (blue line), for the nanoparticle vibrating in its lowest-order breathing mode when it is expanded with a maximum surface displacement of 0.75 nm (green line), and for the vibrating nanoparticle when it is contracted with a maximum surface displacement of 0.75 nm (orange line). Also shown is the measured extinction spectrum for an ensemble of nanoparticles at rest (black points). (b) Calculated magnitude of the electric field at the plasmon resonance frequency for a cross-section through the core–shell nanocube perpendicular to the direction of the incident optical field. The color scale corresponds to the local field magnitude relative to the magnitude of the incident plane wave. (c) Calculated plasmon resonance frequency as a function of vibrational amplitude for the core–shell nanocube vibrating in the lowest-frequency breathing mode at 57 GHz. The amplitude is expressed in terms of the displacement of the corner of the cube. Positive displacements correspond to the expansion of the particle, and negative displacements correspond to contraction. (d) Calculated plasmon resonance frequency as a function of vibrational amplitude for the core–shell nanocube vibrating in the second-lowest breathing mode at 78 GHz. The amplitude is expressed in terms of the displacement at the center of the face of the cube.

particles is not expected to lead to a bimodal size distribution. A low-frequency mode has also been reported for the relative motion of two metal nanostructures in mechanical contact with one another.⁵² However, we study the nanoparticles as a dilute, stable colloidal suspension and do not see evidence of aggregation. Any instability of the solution would lead to the formation of larger aggregates with different vibrational frequencies (depending on the number of particles in the aggregates) and not just to dimers. Moreover, mechanical coupling between particles is expected to lead to shifts in their vibrational frequencies, and the observed frequencies are in good agreement with the calculated frequencies for isolated particles. We therefore propose instead that the observed low-frequency oscillation in the TA measurements is a difference-frequency signal due to a nonlinear mixing process.

In the TA measurements, the nanoparticle vibrations are impulsively rather than continuously driven, ruling out the possibility that parametric processes are responsible for the observed frequency mixing. It is also unlikely that mechanical nonlinearities are responsible for the observed mixing, because the silver and gold that make up the particles and the water that surrounds the particles are known to have a linear mechanical response, especially for the small vibrational amplitudes involved (less than 1 nm). Geometrical nonlinearities are likewise unlikely because of the compact geometry of the nanoparticles and the small vibrational amplitudes. Moreover, finite-element calculations show a linear displacement for all points within and on the surface of the nanoparticles, regardless of the vibrational amplitude, ruling out geometric nonlinearities (see Figure S2).

We propose instead that the observed frequency mixing is due to a nonlinear transduction between the optical signal and the mechanical vibration. In a simple analogy, if the vibration

of the nanoparticle can be approximated using a single displacement coordinate δ , then the total displacement due to the combination of two vibrational modes at frequencies f_1 and f_2 can be written as a linear combination of the displacements, δ_1 and δ_2 , corresponding to each of those frequencies: $\delta = \delta_1 \cos(2\pi f_1 t) + \delta_2 \cos(2\pi f_2 t)$. If, in addition, the optical signal is a nonlinear function of the total displacement, $\Delta A = A^{(1)}\delta + A^{(2)}\delta^2 + \dots$, then the signal will have components at frequencies f_1 , f_2 , $2f_1$, $2f_2$, $(f_1 + f_2)$, and $(f_1 - f_2)$. This frequency generation requires only that the signal is nonlinear in the total displacement and can thus arise from a nonlinearity in either one of the modes alone. The difference-frequency signal will oscillate significantly more slowly than any of the others and will thus be more readily detectable in the time-domain measurements. The sum-frequency and second-harmonic signals, in contrast, have periods that are comparable to the step size between data points along the time axis in our measurements and thus are not readily detectable in our experiments. We note that this simple one-dimensional treatment is meant only to illustrate the frequency-mixing concept and does not capture the complex spatial profile of the particle undergoing deformation due to multiple modes simultaneously or how this deformation translates into an optical signal.

The nanoparticle vibrations affect their optical absorption by shifting the plasmon resonance frequency. Previous calculations for different nanoparticle geometries have indicated that the shift in plasmon frequency is linear with respect to the vibrational amplitude.²⁵ Even for this linear shift in resonance frequency, the absorption at a given wavelength could have a nonlinear dependence on vibrational amplitude due to the curvature of the absorption spectrum around the resonance. Since this effect has not been previously observed to lead to

nonlinear mixing in optical measurements of vibrating nanoparticles, we propose that a different nonlinearity is operational in the core–shell nanoparticles studied here; specifically, the shift in plasmon frequency has a nonlinear dependence on the vibrational amplitude.

To support this hypothesis of nonlinear transduction, we calculate the change in the extinction spectrum for a core–shell nanocube as it undergoes vibrations.⁵³ The finite-element simulations of the mechanical vibrational modes, described above, are used to calculate the deformation of the particle as it undergoes vibrations. Local strains due to this deformation are used, in turn, to calculate local changes in the dielectric function of the nanoparticle.²⁵ The position-dependent dielectric function and the deformed particle geometry are then used as the input for a finite-element calculation of the optical extinction cross-section of the particle. (Details of the calculations are given in the [Supporting Information](#).)

As shown in [Figure 4a](#), the calculated absorption spectrum of a nanoparticle at rest reproduces well the experimentally measured absorption spectrum for the ensemble of the nanoparticles. The spectrum is dominated by a plasmon resonance with a peak close to 450 nm; [Figure 4b](#) shows the localized electric fields associated with excitation of this resonance. As the nanoparticle expands and contracts, the plasmon resonance shifts to longer and shorter wavelengths; examples of the shifted spectra are shown in [Figure 4a](#). The corresponding transient spectra will simply be the difference between the shifted and unshifted extinction spectra. [Figure 4c,d](#) shows the magnitudes of the calculated plasmon resonance shifts as a function of amplitude of the nanoparticle vibration; here, the amplitude is defined as the displacement of the point on the surface of the nanoparticle that moves the furthest from its equilibrium position. The calculated range of vibrational amplitudes is chosen to correspond to the order of magnitude of the vibrational amplitudes that occur experimentally (see the [SI Methods](#) section). The larger shift due to the lower-frequency breathing mode is linear with respect to the amplitude of the vibration. In contrast, the smaller shift due to the higher-frequency mode is highly nonlinear, even reversing slope for larger amplitudes. This nonlinearity provides a potential mechanism for the observed frequency mixing in the TA signal.

We note that this nonlinearity arises only if we consider the local strain distribution within the nanoparticle and the resulting local changes in dielectric function (in contrast to our previous calculations, where we considered only average changes in dielectric function and saw only linear peak shifts for various nanoparticle geometries²⁵). This suggests that the nonlinear transduction is related to the nonuniform strain distribution within the vibrating nanoparticle. We also note that this nonlinear transduction appears to be specific to the geometry of the core–shell nanoparticle studied and is not present in higher-symmetry particles such as nanospheres or nanorods.

In summary, we have observed a low-frequency oscillation in transient-absorption measurements on isolated metal nanoparticles in solution. The frequency of the oscillation is approximately equal to the difference between the frequencies of the two lowest-order breathing modes of the particle, suggesting a nonlinear mixing of these mechanical frequencies. Finite-element simulations suggest that this mixing is due to a nonlinearity in the transduction of the mechanical vibrations into a measurable optical signal.

Although our calculations support this interpretation in terms of nonlinear optical transduction, we cannot definitively rule out other potential mechanisms. In particular, the interface between the octahedral gold core and the cubic silver shell may introduce mechanical nonlinearities due to the small lattice mismatch between the two materials. Alternatively, recent calculations have indicated that highly nonuniform, time-dependent temperature distributions are present in vibrating metal nanoparticles,⁵⁴ and these nonlinear temperature effects may couple to the vibrations through the temperature-dependent mechanical properties of the metals. Nonetheless, the finite-element calculations clearly indicate a highly nonlinear dependence of the nanoparticle extinction spectrum on the amplitude of its vibration, which suggests a novel mechanism for frequency mixing in the optical measurements.

Future measurements on nanoparticles with different structures should help rule out alternative mechanisms as well as any possibility that the observed signal arises from unexpected mechanical coupling among the nanoparticles. It may also be possible to design nanoparticle geometries that maximize the nonlinear transduction, guided by finite-element simulations. This will open up new possibilities for nonlinear frequency mixing at GHz–THz frequencies, including side-band generation, acoustical frequency-comb generation, and high-efficiency frequency mixing.

■ ASSOCIATED CONTENT

Supporting Information

The Supporting Information is available free of charge at <https://pubs.acs.org/doi/10.1021/acs.nanolett.2c01339>.

Details of nanoparticle synthesis, time-resolved measurements, finite element modeling, principal component analysis, additional TA data, and additional results of PCA ([PDF](#))

■ AUTHOR INFORMATION

Corresponding Authors

Aftab Ahmed – Department of Electrical Engineering, California State University, Long Beach, California 90840, United States; Email: aftab@csulb.edu

Jeffrey R. Guest – Center for Nanoscale Materials, Argonne National Laboratory, Lemont, Illinois 60439, United States; orcid.org/0000-0002-9756-8801; Email: jrguest@anl.gov

Matthew Pelton – Department of Physics, University of Maryland, Baltimore County, Baltimore, Maryland 21250, United States; orcid.org/0000-0002-6370-8765; Email: mpelton@umbc.edu

Authors

Rachel Gelfand – Department of Physics, University of Maryland, Baltimore County, Baltimore, Maryland 21250, United States

S. David Storm – Department of Physics, University of Maryland, Baltimore County, Baltimore, Maryland 21250, United States; orcid.org/0000-0002-1480-6959

Anna Lee – Department of Chemistry and Biochemistry, University of Minnesota, Duluth, Minnesota 55812, United States

Anna Klinkova – Department of Chemistry, University of Waterloo, Waterloo, Ontario N2L 3G1, Canada; orcid.org/0000-0003-0337-0579

Complete contact information is available at:
<https://pubs.acs.org/10.1021/acs.nanolett.2c01339>

Author Contributions

A.A., J.R.G., and M.P. conceived the project. A.A. performed transient-absorption measurements. R.G. performed mechanical and electromagnetic finite-element calculations. S.D.S. performed principal component analysis of the data. A.L. and A.A. performed mechanical finite-element calculations. A.K. synthesized the core-shell metal nanoparticles. J.R.G. supervised the experimental measurements. M.P. supervised data analysis and finite-element simulations. A.A. and M.P. wrote the manuscript. All authors contributed to the discussions and interpretation of the results. All authors have given approval to the final version of the manuscript.

Notes

The authors declare no competing financial interest.

ACKNOWLEDGMENTS

Work performed at the Center for Nanoscale Materials, a U.S. Department of Energy Office of Science User Facility, was supported by the U.S. DOE, Office of Basic Energy Sciences, under Contract No. DE-AC02-06CH11357. A.A. acknowledges funding from the U.S. National Science Foundation under LEAPS-MPS Award No. 2137952 and LDRD funding from Argonne National Laboratory, provided by the Director, Office of Science, of the U.S. Department of Energy under Contract No. DE-AC02-06CH11357. A.K. acknowledges support from the University of Waterloo and the Natural Sciences and Engineering Research Council of Canada. M.P. and R.G. acknowledge funding from the U.S. National Science Foundation under grant DMR-1554895.

REFERENCES

- (1) Lifshitz, R.; Cross, M. C. Nonlinear dynamics of nanomechanical and micromechanical resonators. In *Reviews of Nonlinear Dynamics and Complexity*; Wiley, 2008.
- (2) Rhoads, J. F.; Shaw, S. W.; Turner, K. L. Nonlinear Dynamics and Its Applications in Micro- and Nanoresonators. *J. Dyn. Syst. Meas. Control* **2010**, 132 (3), 034001.
- (3) Postma, H. W. Ch.; Kozinsky, I.; Husain, A.; Roukes, M. L. Dynamic Range of Nanotube- and Nanowire-Based Electromechanical Systems. *Appl. Phys. Lett.* **2005**, 86 (22), 223105.
- (4) Rugar, D.; Grütter, P. Mechanical Parametric Amplification and Thermomechanical Noise Squeezing. *Phys. Rev. Lett.* **1991**, 67 (6), 699–702.
- (5) Eichler, A.; del Álamo Ruiz, M.; Plaza, J. A.; Bachtold, A. Strong Coupling between Mechanical Modes in a Nanotube Resonator. *Phys. Rev. Lett.* **2012**, 109 (2), 025503.
- (6) Westra, H. J. R.; Poot, M.; van der Zant, H. S. J.; Venstra, W. J. Nonlinear Modal Interactions in Clamped-Clamped Mechanical Resonators. *Phys. Rev. Lett.* **2010**, 105 (11), 117205.
- (7) Mahboob, I.; Wilmar, Q.; Nishiguchi, K.; Fujiwara, A.; Yamaguchi, H. Wide-Band Idler Generation in a GaAs Electro-mechanical Resonator. *Phys. Rev. B* **2011**, 84 (11), 113411.
- (8) Mahboob, I.; Wilmar, Q.; Nishiguchi, K.; Fujiwara, A.; Yamaguchi, H. Tuneable Electromechanical Comb Generation. *Appl. Phys. Lett.* **2012**, 100 (11), 113109.
- (9) Cao, L. S.; Qi, D. X.; Peng, R. W.; Wang, M.; Schmelcher, P. Phononic Frequency Combs through Nonlinear Resonances. *Phys. Rev. Lett.* **2014**, 112 (7), 075505.
- (10) Chen, C.; Zanette, D. H.; Guest, J. R.; Czaplewski, D. A.; López, D. Self-Sustained Micromechanical Oscillator with Linear Feedback. *Phys. Rev. Lett.* **2016**, 117 (1), 017203.
- (11) Antonio, D.; Czaplewski, D. A.; Guest, J. R.; López, D.; Arroyo, S. I.; Zanette, D. H. Nonlinearity-Induced Synchronization Enhancement in Micromechanical Oscillators. *Phys. Rev. Lett.* **2015**, 114 (3), 034103.
- (12) Wheaton, S.; Gelfand, R. M.; Gordon, R. Probing the Raman-Active Acoustic Vibrations of Nanoparticles with Extraordinary Spectral Resolution. *Nat. Photonics* **2015**, 9 (1), 68–72.
- (13) Portales, H.; Goubet, N.; Saviot, L.; Adichtchev, S.; Murray, D. B.; Mermet, A.; Duval, E.; Pileni, M.-P. Probing Atomic Ordering and Multiple Twinning in Metal Nanocrystals through Their Vibrations. *Proc. Natl. Acad. Sci. U. S. A.* **2008**, 105 (39), 14784–14789.
- (14) Weitz, D. A.; Gramila, T. J.; Genack, A. Z.; Gersten, J. I. Anomalous Low-Frequency Raman Scattering from Rough Metal Surfaces and the Origin of Surface-Enhanced Raman Scattering. *Phys. Rev. Lett.* **1980**, 45 (5), 355–358.
- (15) Gersten, J. I.; Weitz, D. A.; Gramila, T. J.; Genack, A. Z. Inelastic Mie Scattering from Rough Metal Surfaces: Theory and Experiment. *Phys. Rev. B* **1980**, 22 (10), 4562–4571.
- (16) Large, N.; Saviot, L.; Margueritat, J.; Gonzalo, J.; Afonso, C. N.; Arbouet, A.; Langot, P.; Mlayah, A.; Aizpurua, J. Acousto-Plasmonic Hot Spots in Metallic Nano-Objects. *Nano Lett.* **2009**, 9 (11), 3732–3738.
- (17) Fujii, M.; Nagareda, T.; Hayashi, S.; Yamamoto, K. Low-Frequency Raman Scattering from Small Silver Particles Embedded in SiO₂ Thin Films. *Phys. Rev. B* **1991**, 44 (12), 6243–6248.
- (18) Wu, J.; Xiang, D.; Gordon, R. Characterizing Gold Nanorods in Aqueous Solution by Acoustic Vibrations Probed with Four-Wave Mixing. *Opt. Express* **2016**, 24 (12), 12458–12465.
- (19) Xiang, D.; Gordon, R. Nanoparticle Acoustic Resonance Enhanced Nearly Degenerate Four-Wave Mixing. *ACS Photonics* **2016**, 3 (8), 1421–1425.
- (20) Hartland, G. V. Optical Studies of Dynamics in Noble Metal Nanostructures. *Chem. Rev.* **2011**, 111 (6), 3858–3887.
- (21) Crut, A.; Maioli, P.; Del Fatti, N.; Vallée, F. Acoustic Vibrations of Metal Nano-Objects: Time-Domain Investigations. *Phys. Rep.* **2015**, 549, 1–43.
- (22) Major, T. A.; Lo, S. S.; Yu, K.; Hartland, G. V. Time-Resolved Studies of the Acoustic Vibrational Modes of Metal and Semiconductor Nano-Objects. *J. Phys. Chem. Lett.* **2014**, 5 (5), 866–874.
- (23) Hodak, J. H.; Henglein, A.; Hartland, G. V. Photophysics of Nanometer Sized Metal Particles: Electron-phonon Coupling and Coherent Excitation of Breathing Vibrational Modes. *J. Phys. Chem. B* **2000**, 104 (43), 9954–9965.
- (24) Voisin, C.; Del Fatti, N.; Christofilos, D.; Vallée, F. Ultrafast Electron Dynamics and Optical Nonlinearities in Metal Nanoparticles. *J. Phys. Chem. B* **2001**, 105 (12), 2264–2280.
- (25) Ahmed, A.; Pelton, M.; Guest, J. R. Understanding How Acoustic Vibrations Modulate the Optical Response of Plasmonic Metal Nanoparticles. *ACS Nano* **2017**, 11 (9), 9360–9369.
- (26) Hartland, G. V. Measurements of the Material Properties of Metal Nanoparticles by Time-Resolved Spectroscopy. *Phys. Chem. Chem. Phys.* **2004**, 6 (23), 5263–5274.
- (27) Pelton, M.; Sader, J. E.; Burgin, J.; Liu, M.; Guyot-Sionnest, P.; Goszola, D. Damping of Acoustic Vibrations in Gold Nanoparticles. *Nat. Nanotechnol.* **2009**, 4 (8), 492–495.
- (28) Pelton, M.; Chakraborty, D.; Malachosky, E.; Guyot-Sionnest, P.; Sader, J. E. Viscoelastic Flows in Simple Liquids Generated by Vibrating Nanostructures. *Phys. Rev. Lett.* **2013**, 111 (24), 244502.
- (29) Yu, K.; Major, T. A.; Chakraborty, D.; Devadas, M. S.; Sader, J. E.; Hartland, G. V. Compressible Viscoelastic Liquid Effects Generated by the Breathing Modes of Isolated Metal Nanowires. *Nano Lett.* **2015**, 15 (6), 3964–3970.
- (30) Yu, K.; Yang, Y.; Wang, J.; Hartland, G. V.; Wang, G. P. Nanoparticle-Fluid Interactions at Ultrahigh Acoustic Vibration Frequencies Studied by Femtosecond Time-Resolved Microscopy. *ACS Nano* **2021**, 15 (1), 1833–1840.
- (31) Uthe, B.; Collis, J. F.; Madadi, M.; Sader, J. E.; Pelton, M. Highly Spherical Nanoparticles Probe Gigahertz Viscoelastic Flows of

Simple Liquids without the No-Slip Condition. *J. Phys. Chem. Lett.* **2021**, *12* (18), 4440–4446.

(32) Chakraborty, D.; Uthe, B.; Malachosky, E. W.; Pelton, M.; Sader, J. E. Viscoelasticity Enhances Nanometer-Scale Slip in Gigahertz-Frequency Liquid Flows. *J. Phys. Chem. Lett.* **2021**, *12* (13), 3449–3455.

(33) Xiang, D.; Wu, J.; Rottler, J.; Gordon, R. Threshold for Terahertz Resonance of Nanoparticles in Water. *Nano Lett.* **2016**, *16* (6), 3638–3641.

(34) Hsueh, C.-C.; Gordon, R.; Rottler, J. Dewetting during Terahertz Vibrations of Nanoparticles. *Nano Lett.* **2018**, *18* (2), 773–777.

(35) Gambetta, A.; Manzoni, C.; Menna, E.; Meneghetti, M.; Cerullo, G.; Lanzani, G.; Tretiak, S.; Piryatinski, A.; Saxena, A.; Martin, R. L.; Bishop, A. R. Real-Time Observation of Nonlinear Coherent Phonon Dynamics in Single-Walled Carbon Nanotubes. *Nat. Phys.* **2006**, *2* (8), 515–520.

(36) Khairullina, E.; Mosina, K.; Choueiri, R. M.; Paradis, A. P.; Petruk, A. A.; Sciaini, G.; Krivoschapkina, E.; Lee, A.; Ahmed, A.; Klinkova, A. An Aligned Octahedral Core in a Nanocage: Synthesis, Plasmonic, and Catalytic Properties. *Nanoscale* **2019**, *11* (7), 3138–3144.

(37) Tao, A. R.; Habas, S.; Yang, P. Shape Control of Colloidal Metal Nanocrystals. *Small* **2008**, *4* (3), 310–325.

(38) Wiley, B. J.; Im, S. H.; Li, Z.-Y.; McLellan, J.; Siekkinen, A.; Xia, Y. Maneuvering the Surface Plasmon Resonance of Silver Nanostructures through Shape-Controlled Synthesis. *J. Phys. Chem. B* **2006**, *110* (32), 15666–15675.

(39) Petrova, H.; Lin, C.-H.; de Liejer, S.; Hu, M.; McLellan, J. M.; Siekkinen, A. R.; Wiley, B. J.; Marquez, M.; Xia, Y.; Sader, J. E.; Hartland, G. V. Time-Resolved Spectroscopy of Silver Nanocubes: Observation and Assignment of Coherently Excited Vibrational Modes. *J. Chem. Phys.* **2007**, *126* (9), 094709.

(40) Staleva, H.; Hartland, G. V. Vibrational Dynamics of Silver Nanocubes and Nanowires Studied by Single-Particle Transient Absorption Spectroscopy. *Adv. Funct. Mater.* **2008**, *18* (23), 3809–3817.

(41) Staleva, H.; Hartland, G. V. Transient Absorption Studies of Single Silver Nanocubes. *J. Phys. Chem. C* **2008**, *112* (20), 7535–7539.

(42) Hartland, G. V. Coherent Excitation of Vibrational Modes in Metallic Nanoparticles. *Annu. Rev. Phys. Chem.* **2006**, *57* (1), 403–430.

(43) Pelton, M.; Aizpurua, J.; Bryant, G. Metal-Nanoparticle Plasmonics. *Laser Photonics Rev.* **2008**, *2* (3), 136–159.

(44) Del Fatti, N.; Voisin, C.; Christofilos, D.; Vallée, F.; Flytzanis, C. Acoustic Vibration of Metal Films and Nanoparticles. *J. Phys. Chem. A* **2000**, *104* (18), 4321–4326.

(45) Stoll, T.; Maioli, P.; Crut, A.; Burgin, J.; Langot, P.; Pellarin, M.; Sánchez-Iglesias, A.; Rodríguez-González, B.; Liz-Marzán, L. M.; Del Fatti, N.; Vallée, F. Ultrafast Acoustic Vibrations of Bimetallic Nanoparticles. *J. Phys. Chem. C* **2015**, *119* (3), 1591–1599.

(46) Crut, A.; Juvé, V.; Mongin, D.; Maioli, P.; Del Fatti, N.; Vallée, F. Vibrations of Spherical Core-Shell Nanoparticles. *Phys. Rev. B* **2011**, *83* (20), 205430.

(47) Dacosta Fernandes, B.; Spuch-Calvar, M.; Baida, H.; Tréguer-Delapierre, M.; Oberlé, J.; Langot, P.; Burgin, J. Acoustic Vibrations of Au Nano-Bipyramids and Their Modification under Ag Deposition: A Perspective for the Development of Nanobalances. *ACS Nano* **2013**, *7* (9), 7630–7639.

(48) Sader, J. E.; Hartland, G. V.; Mulvaney, P. Theory of Acoustic Breathing Modes of Core-shell Nanoparticles. *J. Phys. Chem. B* **2002**, *106* (6), 1399–1402.

(49) Wang, L.; Kiya, A.; Okuno, Y.; Niidome, Y.; Tamai, N. Ultrafast Spectroscopy and Coherent Acoustic Phonons of Au–Ag Core–Shell Nanorods. *J. Chem. Phys.* **2011**, *134* (5), 054501.

(50) Hodak, J. H.; Henglein, A.; Hartland, G. V. Coherent Excitation of Acoustic Breathing Modes in Bimetallic Core-shell Nanoparticles. *J. Phys. Chem. B* **2000**, *104* (21), 5053–5055.

(51) Yu, S.; Zhang, J.; Tang, Y.; Ouyang, M. Engineering Acoustic Phonons and Electron–Phonon Coupling by the Nanoscale Interface. *Nano Lett.* **2015**, *15* (9), 6282–6288.

(52) Wang, J.; Yu, K.; Yang, Y.; Hartland, G. V.; Sader, J. E.; Wang, G. P. Strong Vibrational Coupling in Room Temperature Plasmonic Resonators. *Nat. Commun.* **2019**, *10* (1), 1527.

(53) Saison-Francioso, O.; Lévêque, G.; Akjouj, A. Numerical Modeling of Acousto–Plasmonic Coupling in Metallic Nanoparticles. *J. Phys. Chem. C* **2020**, *124*, 12120.

(54) Lindley, S. A.; An, Q.; Goddard, W. A.; Cooper, J. K. Spatiotemporal Temperature and Pressure in Thermoplasmonic Gold Nanosphere–Water Systems. *ACS Nano* **2021**, *15*, 6276–6288.